Chapter 19
Transpiration in Forest Ecosystems

Tomo'omi Kumagai

19.1 Introduction

Water molecules having sufficient kinetic energy escape from the surface of liquid water to the air, while water molecules in vapor form return from the air to a liquid state. When the rates of escaping and returning water molecules are the same, the process is said to be in an equilibrium status with no net evaporation from the water surface. If air flow carries away many of the molecules that escape from the liquid surface and if this rate of loss is greater than the rate of molecules returning to the surface net evaporation occurs.

Ohm's law describes that the electric current in a circuit is directly proportional to the voltage and inversely proportional to the resistance of the circuit. Mass transport between a surface and its surroundings is analogous with Ohm's law, substituting the mass flow and concentration difference for the current and voltage, respectively. The concentration difference is specified as that between the surface and the overlying air, while the resistance represents a force that reduces the rate of mass flow. Here, we consider evaporation rate (E) from the water surface to the air as a mass flow by assuming an equilibrium status in a thin layer adjacent to the water surface, where the water vapor concentration can be described as the saturation value (C_{WS}) at the surface temperature (T_{s}) to give

$$E = \frac{C_{\mathrm{WS}}(T_{\mathrm{s}}) - C_{\mathrm{Wa}}}{r_{\mathrm{W}}} = g_{\mathrm{W}}[C_{\mathrm{WS}}(T_{\mathrm{s}}) - C_{\mathrm{Wa}}], \tag{19.1}$$

where r_{W} is the resistance of the evaporation, g_{W} is the conductance, the reciprocal of the resistance, and C_{Wa} is the water vapor concentration in the air.

When considering transpiration from plant leaves the evaporating sites are found on the surface of leave's mesophyll cells, and the water vapor concentration at the cell surface can be described as $C_{\mathrm{WS}}(T_{\mathrm{s}})$ because the cell surface is thought to be "perfectly wet" (Fig. 19.1). The pathway of transpiration is from the cell surfaces to the atmosphere via a stoma, and thus total resistance, r_{W}, consists of stomatal (r_{S}) and boundary layer (r_{a}) resistances in series. It should be noted that the reciprocal of the total conductance, g_{W}, is the sum of the reciprocals of the component conductances, i.e., stomatal (g_{S}) and boundary layer (g_{a}) conductances:

D.F. Levia et al. (eds.), *Forest Hydrology and Biogeochemistry: Synthesis of Past Research and Future Directions*, Ecological Studies 216,
DOI 10.1007/978-94-007-1363-5_19,

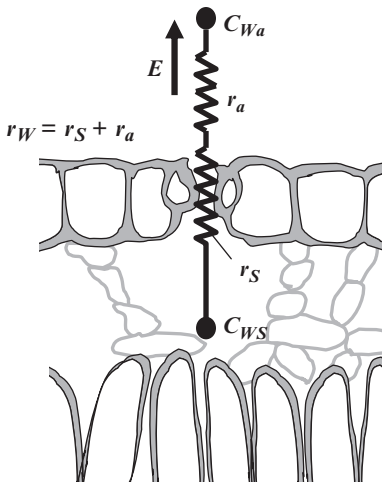

Fig. 19.1 A pathway of transpiration (E) from mesophyll cell surface to the atmosphere, showing the stomatal (r_S) and boundary layer (r_a) resistances. Note that the total resistance (r_W) is the sum of r_S and r_a resistances

$$\frac{1}{g_W} = \frac{1}{g_S} + \frac{1}{g_a}. \tag{19.2}$$

Equations (19.1) and (19.2) represent the basic formulae of transpiration at both the individual leaf and canopy scales. Thus, determination of g_S and g_a is critical for estimating transpiration at both scales.

19.2 Boundary Layer (g_a) and Stomatal (g_S) Conductance

The velocity of microwind flowing over a leaf decreases toward the leaf surface due to the friction between the surface and the air and the air viscosity. The zone adjacent to the surface, where the airflow is laminar and mass transfer can be described using molecular diffusivity, is referred to as the boundary layer.

The boundary layer conductance of any mass for one surface of a rectangular, flat plate with the downwind width (d_m) was developed using the molecular diffusivity for species j (D_j), Reynolds number, and Schmidt number, and also assuming that wind is naturally turbulent, to give

$$g_a = 0.93\rho_a D_j^{2/3} v^{1/6} \sqrt{\frac{u}{d_m}}, \tag{19.3}$$

where ρ_a is the air density, v is the kinematic viscosity, and u is the wind velocity of the free stream. Using the molecular diffusivity for water vapor (19.3) becomes the conductance in air for water vapor (mol m^{-2} s^{-1}) (see Campbell and Norman 1998):

$$g_a = 0.147\sqrt{\frac{u}{d_m}}. \tag{19.4}$$

It should be noted that (19.3) and (19.4) also suggest that the thickness of the boundary layer over the surface decreases in proportion to the increasing square roots of u and $1/d_m$.

Since the water vapor concentration gradient between the stomatal cavity and the air surrounding the leaf is several hundred times greater than the CO_2 concentration gradient, opening stomata for carbon gain is accompanied by much water loss from the plant body via transpiration. Wong et al. (1979) have shown that plants tend to adjust the degree of stomata openness in order to maintain a constant ratio between the intercellular CO_2 concentration (C_{Ci}) and the CO_2 concentration of air inside the leaf boundary layer (C_{Cs}) for a wide range of environmental conditions, but that this relationship varies from species to species. Many researchers have related the net assimilation rate (A) to g_S. One widely used g_S model is the Ball–Berry model (Ball et al. 1987; Collatz et al. 1991), which is given by

$$g_{sC} = m\frac{Ah_s}{C_{Cs}} + b, \tag{19.5}$$

where g_{sC} is the stomatal conductance for CO_2 and h_s is the relative humidity of air inside the leaf boundary layer. m and b are, respectively, the slope and intercept obtained by linear regression analysis of data from leaf-level gas exchange measurements, i.e., g_{sC} vs. Ah_s/C_{Cs} plots. The stomatal conductance for water vapor is obtained from $g_S = 1.6g_{sC}$, where 1.6 is the ratio of the diffusivities of CO_2 and water vapor in air.

However, it is widely accepted that stomata respond to the leaf surface humidity deficit (D_s) rather than to h_s. Furthermore, since A approaches zero when C_{Cs} approaches the CO_2 compensation point (Γ), (19.5) cannot describe stomatal behavior at low CO_2 concentrations. Leuning (1995) replaced h_s and C_{Cs} in (19.5) with a vapor pressure deficit correction function $f(D_s)$ and $C_{Cs} - \Gamma$, respectively,

$$g_{sC} = a_{sC}\frac{Af(D_s)}{C_{Cs} - \Gamma} + g_{sC0}, \quad f(D_s) = \left(1 + \frac{D_s}{D_0}\right)^{-1}, \tag{19.6}$$

where g_{sC0} is a residual stomatal conductance (as A approaches zero when light intensity approaches zero), and a_{sC} and D_0 are empirical parameters.

The net assimilation rate, A, can be described as

$$A = g_{sC}(C_{Cs} - C_{Ci}) \tag{19.7}$$

and reduces to

$$C_{Ci} = C_{Cs} - \frac{A}{g_{sC}}. \tag{19.8}$$

Equation (19.8) describes supplying CO_2 to the intracellular photosynthetic site with constraint by stomatal openness (g_{sC}: (19.6)) (Fig. 19.2). On the other hand, A can be described as a function of C_{Ci}. Thus, the intersection of these two function curves gives the "operating point," which denotes that stomata close or open to balance the supply of CO_2 via g_S with the demand of CO_2 by A (Fig. 19.2).

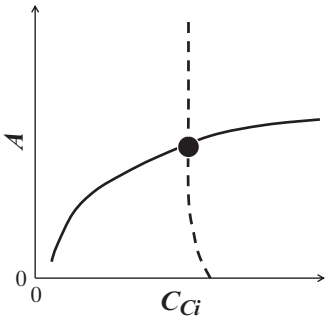

Fig. 19.2 Assimilation rate (A) as a function of intercellular CO_2 concentration (C_{Ci}) at some light and leaf temperature level (*solid line*), showing the photosynthetic demand function. The supply-constraint function (Eq. 19.8) by taking (Eq. 19.6) into consideration (*broken line*) is also shown for some environmental variables and empirical constants. The *solid circle* denotes the "operating point" of the leaf that is given by the intersection of the demand and supply-constraint curves. Note the fundamental concept provided by Leuning (1995)

Equations (19.5) and (19.6) are, in reality, difficult to solve. For example, A as a function of C_{Ci} is dependent on complex biochemical reactions in the intracellular photosynthetic site of the leaf, and intrinsically, A should be determined using a biochemical photosynthesis model (see Box 19.1: Farquhar et al. 1980). Furthermore, it should be noted that (19.4), (19.5), or (19.6), the photosynthesis model, and the leaf energy budget model for determining the leaf surface temperature must be solved simultaneously.

Another method commonly used for analyzing the response of g_S to governing variables is to use the following series of multiplicative functions (Jarvis 1976):

$$g_S = g_{Smax} f_1(Q_0) f_2(D_s) f_3(T_a) \ldots, \tag{19.9}$$

where g_{Smax} is the maximum g_S, Q_0 is the photosynthetic active radiation (PAR), and T_a is the air temperature. Some particularly useful functions for each of f_1, f_2, and f_3 were proposed and parameters contained in each function can be determined by appropriate nonlinear regression analysis. Oren et al. (1999) focused on the relationship between g_S and D_s by relating g_{Smax} to a reference conductance, g_{Sref}, at $D_s = 1$ kPa as follows:

$$g_S = g_{Sref} - \delta \ln D_s, \tag{19.10}$$

where δ is the sensitivity of g_S to D_s (i.e., $-dg_S/d \ln D_s$). Oren et al. (1999) fit (19.10) to literature data from porometry-based leaf-level measurements and regressed with δ and g_{Sref}. As a result, they found that the interspecific response of δ ($=-dg_S/d \ln D_s$) to g_{Sref} was well correlated with a slope of 0.60 (Fig. 19.3). It should be noted that this result generalized the previous findings that the sensitivity of g_S to D_s increased with g_{Sref} regardless of whether the variation in g_{Sref} was related to some other environmental variables.

Box 19.1. Biochemical Model for Leaf Photosynthesis (Farquhar et al. 1980)

Leaf photosynthesis, A, was computed using the biochemical models of Farquhar et al. (1980) and Collatz et al. (1991):

$$A = \min\{J_E, J_C, J_S\} - R_d,$$

where J_E, J_C, and J_S are the gross rates of photosynthesis limited by the rate of ribulose bisphosphate (RuBP) regeneration through electron transport, RuBP carboxylase-oxygenase (Rubisco) activity, and the export rate of synthesized sucrose, respectively, and R_d is the respiration rate during the day but in the absence of photorespiration. The term $\min\{J_E, J_C, J_S\}$ represents the minimum of J_E, J_C, and J_S.

The formulation and parameterization of J_E, J_C, J_S, and R_d as a function of the PAR absorbed by a leaf, C_{Ci}, and leaf temperature are described in Farquhar et al. (1980), Farquhar and Wong (1984), Collatz et al. (1991), and de Pury and Farquhar (1997). The photosynthesis model constants can be determined according to Badger and Collatz (1977), Farquhar et al. (1980), von Caemmerer et al. (1994), and de Pury and Farquhar (1997). The maximum carboxylation rate when RuBP is saturated (V_{cmax}) and the potential rate of whole-chain electron transport (J_{max}) used in these calculations are expressed as nonlinear functions of temperature using their values at 25°C (J_{max_25} and V_{cmax_25}, respectively); the formulations are given in de Pury and Farquhar (1997). In addition, R_d is expressed as a nonlinear function of temperature using R_d at 25°C (R_{d_25}), which was assumed to be linearly related to V_{cmax_25} (e.g., Collatz et al. 1991). Practically, both J_{max_25} and R_{d_25} are related to V_{cmax_25}, and hence, V_{cmax_25} is the key parameter in the leaf photosynthesis model.

19.3 Hydraulic Constraints on Transpiration

The fundamental driving force of water uptake and transportation in the plant is the water potential. The equation of water flow through a water conducting pathway between the roots and leaves also resembles that of electrical flow in a conducting system, i.e., keeping with the Ohm's law analogy:

$$E = K_L[\psi_s - (\psi_L + h\rho_w g)], \tag{19.11}$$

where K_L is the leaf-specific hydraulic conductance between the soil and leaves, ψ_s and ψ_L are the water potential of soil and leaf, respectively, h is the tree height, ρ_w is the density of water, and g is the gravitational constant. Note that E is

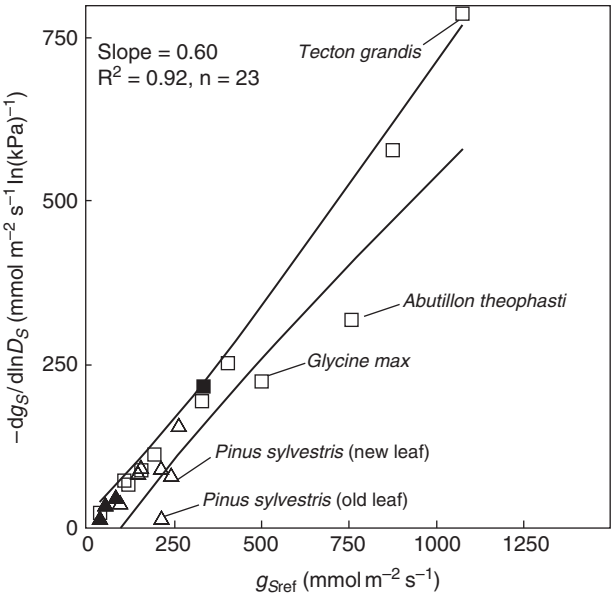

Fig. 19.3 The sensitivity of leaf-level stomatal conductance (g_S) of individual species to increasing vapor pressure deficit at the leaf surface ($-dg_S/d \ln D_s$) as a function of the canopy stomatal conductance at $D_s = 1$ kPa (g_{Sref}). *Lines*: 99% confidence interval. *Symbols*: *triangles*, nonporous; *squares*, diffuse-porous; *full*, boreal species; *shaded*, temperate species; *open*, tropical species. Species outside the confidence interval are shown. From Oren et al. (1999), reproduced with permission

represented as tree transpiration rate per unit leaf area. K_L can be related to sapwood-specific hydraulic conductivity, K_S, as follows:

$$K_L A_L = \frac{1}{h} K_S A_S, \tag{19.12}$$

where A_L and A_S are leaf and sapwood area, respectively. Equation (19.12) denotes that total hydraulic conductance between the roots and leaves increases/decreases with increasing water flow conducting area in the stem cross section, A_S, and soil-to-leaf water flow path length, h, respectively.

The sapwood maintains living cells and can conduct water, while aged xylem changes to the heartwood and loses its water and nutrient transport and storage functions (Fig. 19.4). Anatomically, there are water conducting systems in sapwood (Fig. 19.4) mainly for conifers and broadleaved trees. Conifers have tracheids that serve both mechanical and hydraulic functions, while the broadleaved trees share the role of hydraulic purpose with vessel elements and that of mechanical purpose with fibers. The tracheids are shorter than vessel elements and interlock and exchange water via pits on its side wall. The vessel elements, which are interconnected by simple perforation plates at their ends, are more effective for conducting water.

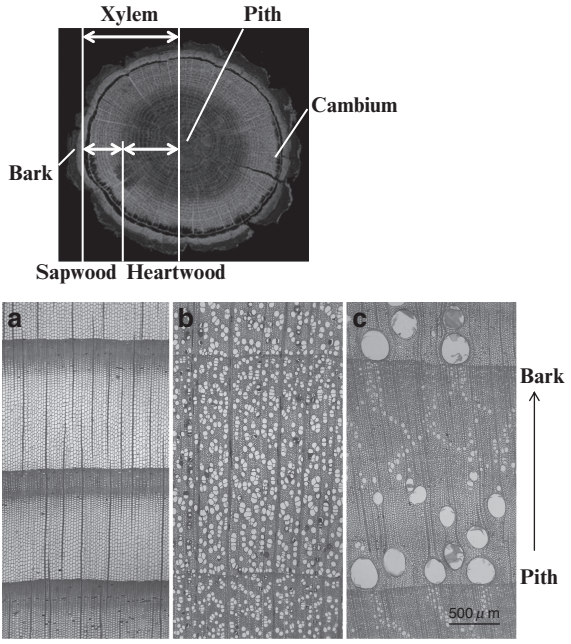

Fig. 19.4 *Upper*: A cross section of an oak stem showing various anatomical components. *Lower*: Xylem cross sections of (**a**) Japanese cedar (conifer), (**b**) cherry (broadleaved tree: diffuse-porous wood), and (**c**) chestnut (broadleaved tree: ring-porous wood). An *arrow* denotes direction from pith to bark. Courtesy of Drs. Y. Utsumi and T. Umebayashi

The sapwood of conifers has systematically arranged cuts of cells (Fig. 19.4a). Round openings found in the sapwood of broadleaved trees are the vessels, and fibers fill nonvessel space (Fig. 19.4b, c). Vessel array characteristics for broadleaved trees are broadly classified as diffuse-porous wood with vessels uniformly distributed throughout the entire sapwood (Fig. 19.4b) and ring-porous wood with larger vessels arranged along the boundary of annual rings (Fig. 19.4c). The spatial variation in sapflow in the stem cross section between those vessel arrays needs to be considered. For example, despite the radial variations in sapflow in the stems of conifers and diffuse-porous wood, ring-porous wood trees tend to have biased sapflow distribution and use mainly current and 2-year-old annual rings for conducting water (see Kumagai et al. 2005; Tateishi et al. 2008; Umebayashi et al. 2008).

A water deficit in the leaf caused by the transpiration lowers its water potential, causing water to move from the xylem to the evaporating cells in the leaf. This reduces the tension or pressure in the xylem sap and produces a water potential gradient in the cohesive hydraulic system of the tree. This pressure is transmitted to the root where water uptake occurs. K_S in (19.12) may be expressed in terms of physical properties of the conducting system in sapwood such as size, density, and connectivity of conduits.

Equation (19.1) is coupled to ψ_L using (19.11) and (19.12) to give

$$g_S = K_S \frac{A_S}{A_L} \frac{1}{D} \frac{1}{h} [\psi_s - (\psi_L + h\rho_w g)], \tag{19.13}$$

where D denotes vapor pressure deficit. In fact, the proportionality 0.60 between δ and g_{Sref} in (19.10) (see Fig. 19.3) was predicted from the examination results of (19.13), which suggested that the 0.60 proportionality regulates the minimum ψ_{L} to prevent excessive xylem cavitation (Oren et al. 1999; Ewers et al. 2005).

19.4 Energy Balance

Radiation incident on the surface (for both of leaf and canopy) is decomposed into solar (short-wave) (R_{s}) and thermal (long-wave) (R_{L}) radiation. All surfaces reflect the incident R_{s} according to the albedo (a_{l}) of that surface, while the remaining R_{s} is either absorbed or transmitted through the surface. Also, following the Stefan–Boltzmann law, all surfaces emit long-wave radiation at a rate proportional to the fourth power of the absolute surface temperature (T_{s}: K). Thus, the total sum of the incident and emitted radiations gives the energy available as net radiation (R_{n}):

$$R_{\mathrm{n}} = R_{\mathrm{sabs}} + R_{\mathrm{Labs}} = (1 - a_{\mathrm{l}})R_{\mathrm{s}} + R_{\mathrm{L}} - \varepsilon\sigma T_{\mathrm{s}}^{4} \tag{19.14}$$

where ε is emissivity compared to a black body, and σ is the Stefan–Boltzmann constant (5.67×10^{-8} W m^{-2} K^{-4}). Intrinsically, the available energy can be represented by the sum of R_{s} and R_{L} absorbed in the body (R_{sabs} and R_{Labs}, respectively, in the middle of (19.14)). When considering the upward surface of the body, R_{sabs} and R_{Labs} can be expressed as $(1 - a_{\mathrm{l}})R_{\mathrm{s}}$ and $R_{\mathrm{L}} - \varepsilon\sigma {T_{\mathrm{s}}}^{4}$, respectively, resulting in the right-hand side of (19.14). Because of comparatively low values of a_{l} and T_{s} at vegetation surfaces, R_{n} above forests tends to have higher values compared to other types of surface such as bare lands (Fig. 19.5a).

The surface (also, for both of leaf and canopy) energy balance is expressed by:

$$R_{\mathrm{n}} = H + \lambda E + G, \tag{19.15}$$

where H and λE are the sensible and latent heat fluxes, respectively, λ is the heat of vaporization of water, and G is the heat storage. It should be noted that when evaporation occurs on the dry leaf or canopy surface, E is the synonym of transpiration. Higher energy partitioning to λE is a characteristic of vegetated surfaces (Fig. 19.5b).

Sensible heat transfer from the leaf surface to the atmosphere is driven by the difference between T_{a} and T_{s} and boundary conductance, and thus, leaf-level H is given by:

$$H = c_{\mathrm{p}} g_{\mathrm{H}} (T_{\mathrm{s}} - T_{\mathrm{a}}), \tag{19.16}$$

where c_{p} is the specific heat of air at constant pressure, and g_{H} is the boundary conductance for heat (mol m^{-2} s^{-1}) and can be expressed in the same form as (19.4), but a coefficient of 0.135 is used instead of 0.147. Assuming that G can be considered negligible, the energy balance on a leaf surface as a function of T_{s} is

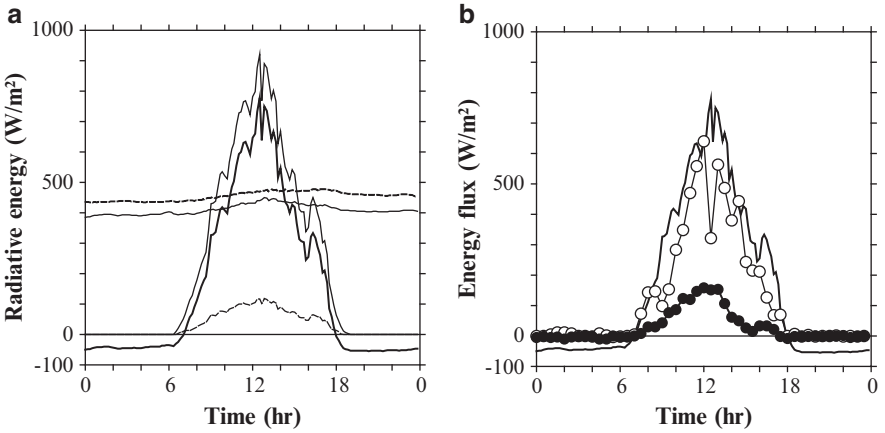

Fig. 19.5 Forest ecosystem energy balance observed in a Bornean tropical rainforest. (**a**) Downward (*thin solid line*) and upward (*thin dashed line*) short-wave radiation, downward (*solid line*) and upward (*dashed line*) long-wave radiation, and the net radiation (*thick solid line*) calculated from balance of those radiation terms. (**b**) Sensible heat flux (*solid circle*), latent heat flux (*open circle*), and the net radiation (*thick solid line*). Note that sensible and latent heat fluxes were measured using the eddy covariance method

described using (19.1) and (19.14) through (19.16). As seen in Box 19.1, T_s is the most critical factor in computing biocatalytic reactions in the photosynthesis model. Thus, it should be noted that while T_s is calculated from the energy balance, T_s simultaneously affects the energy balance via the rate of photosynthesis and the degree of stomatal opening.

When considering the leaf-scale energy balance and photosynthesis within a forest canopy, the radiative transfer through the canopy must be taken into account. Direct beam and diffuse irradiance must, for example, be considered separately due to their different attenuation properties in the canopy. Downward and upward R_L transfer within a canopy follows diffuse irradiance transfer theory, but note that R_L is emitted from any plant body within the canopy. Both direct and diffuse R_s can be further divided into PAR and near-infrared radiation (NIR) according to differential absorption by leaves. Fortunately, approximately half the R_s over the canopy is in the form of PAR, while the other half is in the form of NIR, enabling estimates of R_s penetration inside the canopy. The absorbed PAR or NIR within a canopy layer between z (the height from the ground) and $z + \Delta z$, ΔS, is defined as:

$$\Delta S_b = (1 - \eta - \xi)(1 - P_b)S_b(z + \Delta z), \tag{19.17}$$

$$\Delta S_d^{\downarrow} = (1 - \eta - \xi)(1 - P_d)S_d^{\downarrow}(z + \Delta z), \tag{19.18}$$

$$\Delta S_d^{\uparrow} = (1 - \eta - \xi)(1 - P_d)S_d^{\uparrow}(z), \tag{19.19}$$

where η and ξ are the leaf transmissivity and reflectivity, respectively, for PAR or NIR, and S is PAR or NIR at the given height, while P is the probability of no

contact with the irradiance within that canopy layer. The subscripts b and d denote direct beam and diffuse irradiation, respectively, and superscript arrows denote the direction of the irradiation. Because P is a complex function of the leaf area density, leaf angle distribution, and foliage clumping factor within a given canopy layer and the solar geometric direction (see Kumagai et al. 2006), (19.17) through (19.19) are not readily solved. The total absorbed solar radiation within the canopy layer is then calculated as the sum of the absorbed PAR and NIR, both of which are calculated by (19.17) through (19.19). Sunlit leaves receive the beam and the upward and downward diffuse radiation, while shaded leaves only receive upward and downward diffuse radiation. Therefore, the irradiance absorption and energy balance need to be computed separately for sunlit and shaded leaves (see Kumagai et al. 2006).

19.5 Canopy Transpiration

19.5.1 Multilayer Approach

Vegetation affects the within-canopy microclimate by intercepting radiation, attenuating wind, and distributing a source/sink of mass and energy to each within-canopy position (Fig. 19.6). These source/sink distributions and canopy turbulence form scalar distributions (i.e., air temperature, humidity, and CO_2 concentration) and above-canopy fluxes such as heat, H_2O, and CO_2. It should be noted that in turn these scalar distributions influence the within-canopy microclimate and scalar source/sink strength.

In reality, forest transpiration or H_2O flux above a forest canopy is formed as a result of the above within-canopy processes. Thus, here we focus on a multilayer canopy approach, which explicitly considers three major within-canopy processes: (1) radiative transfer and leaf-scale energy conservation, (2) leaf-scale

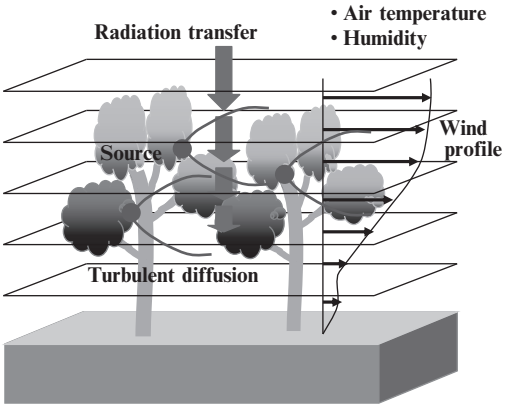

Fig. 19.6 Schematic display of the multilayer Soil–Vegetation–Atmosphere Transfer model for transpiration from a forest ecosystem. Note that the forest canopy is divided into layers for computation of energy and matter exchange between leaves and atmosphere

ecophysiological status for stomatal opening and carbon assimilation, and (3) turbulent diffusion of matter (Baldocchi 1992; Fig. 19.6). For the multilayer approach, the canopy is divided into layers, and all equations describing the within-canopy processes (1–3) (see Kumagai et al. 2006) are solved at each layer. Since the within-canopy processes (1) and (2) have been already introduced, we will proceed to the description of the process (3).

Assuming a steady-state planar-homogeneous and high Reynolds and Peclet numbers flow, and by applying time and horizontal averaging, the scalar continuity and turbulent flux equations for water vapor (q) are (see Katul and Albertson 1999):

$$\frac{\partial \langle \overline{q} \rangle}{\partial t} = 0 = -\frac{\partial \langle \overline{w'q'} \rangle}{\partial z} + S_q, \tag{19.20}$$

$$\frac{\partial \langle \overline{w'q'} \rangle}{\partial t} = 0 = -\langle \overline{w'^2} \rangle \frac{\partial \langle \overline{q} \rangle}{\partial z} - \frac{\partial \langle w'w'q' \rangle}{\partial z} + \left\langle \overline{\frac{p'}{\rho_a}} \overline{\frac{\partial q'}{\partial z}} \right\rangle, \tag{19.21}$$

where the overbar and bracket denote time and horizontal averaging, respectively, prime denotes a departure from the temporal averaging operator, w is the instantaneous vertical velocity, $F_q = \langle \overline{w'q'} \rangle$ is the vertical turbulent flux, t is time, z is height from the ground, p is the static pressure, and ρ_a is the density of air. The three terms on the right-hand side of (19.21) represent respectively the production of turbulent flux due to interactions between the turbulent flow and mean concentration gradient, transport of the turbulent flux, and dissipation as a result of the pressure-scalar interaction. S_q is the source term due to mass release (i.e., transpiration) by the ensemble of leaves within the averaging plane and given by:

$$S_q = \frac{1}{\rho_a} (E_{sl} a_{sl} + E_{sh} a_{sh}), \tag{19.22}$$

where E and a denote the leaf-scale transpiration and the leaf area density in a given layer, respectively, and subscripts sl and sh denote sunlit and shaded leaves, respectively. The last two terms on the right-hand side of (19.21) are unknowns requiring closure approximations, as described by Watanabe (1993). To solve (19.20)–(19.22), including these closure approximations, velocity statistics within the canopy need to be computed. Here, the second-order closure model formulated by Wilson and Shaw (1977) may be applied.

The multilayer model introduced here is parameterized by independently collected ecophysiological measurements and is not calibrated or parameterized by canopy-level flux measurements. The outputs from the model are independently validated using a stand-scale sap flow measurement (see Kumagai et al. 2007, 2008) (Fig. 19.7a). After validation, the model can be used to examine how the matter fluxes above the forest ecosystems are generated, for example, how the canopy structure and physiological traits impact H_2O exchange between the canopy and atmosphere (Fig. 19.7b).

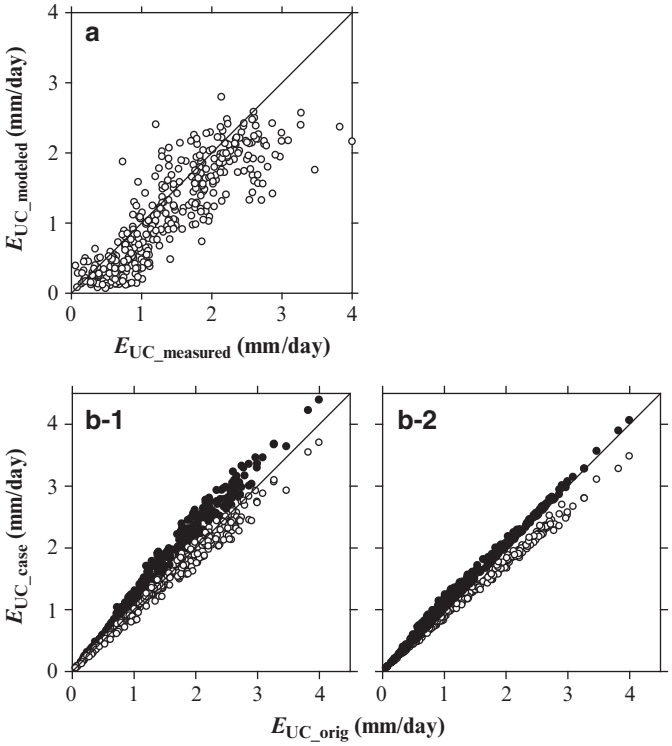

Fig. 19.7 Comparisons (**a**) between measured and modeled (CASE 1) upper-canopy (Japanese cedar trees) transpiration (E_{UC}), and between E_{UC} calculated in CASE 1 (E_{UC_orig}) and in CASEs 2 and 3 (**b-1**) and in CASEs 4 and 5 (**b-2**) (E_{UC_case}). Canopy transpiration was calculated (CASE 1) considering seasonal variations in LAI and the maximum Rubisco catalytic capacity (V_{cmax}), setting LAI as the maximum value (CASE 2: *solid circle*) and the minimum value (CASE 3: *open circle*), and setting V_{cmax} as the maximum value (CASE 4: *solid circle*) and the minimum value (CASE 5: *open circle*) in the study period

19.5.2 Big-Leaf Approach

Assuming that the vegetation in which matter and energy are exchanged can be represented as a single layer, i.e., "big leaf," (19.1) and (19.16) are rearranged using surface or canopy conductance G_S and aerodynamic conductance G_a instead of using g_S and g_a (assuming $= g_H$), respectively.

When leaf area index (LAI) is >3 (see Kelliher et al. 1995) or G_S is derived from transpiration measurement for individual plant, e.g., sap flow measurements, G_S represents mean stomatal conductance within a canopy and is called the canopy conductance. This bulk conductance is usually related to physiological control, and therefore, described using (19.5), (19.6), (19.9), and (19.10), which are the functions for describing leaf-level g_S. At LAI $<$ 3 (see Kelliher et al. 1995) and/or when the water vapor flux is measured above a canopy, e.g., by the eddy covariance method, evaporation from the floor vegetation or the soil surface contributes greatly to G_S.

In case of the "big-leaf" approach, the concept of leaf-level g_a is developed into the conductance between the canopy surface and the atmosphere above the canopy, namely, the aerodynamic conductance G_a. From the equation for wind velocity profile above the canopy under adiabatic condition, G_a can be derived as follows:

$$G_a = \frac{\kappa^2 u}{(\ln(z - d/z_0))^2}, \tag{19.23}$$

where z is the height of wind speed observation, u is the wind speed at z, κ is the von Karman's constant (0.4), d is the zero-plane displacement, and z_0 is the roughness length. For computing G_a, the d and z_0 are usually set as 2/3 and 1/10 of the canopy height, respectively. It should be noted that the G_a represents the conductance of the atmospheric surface layer between a height of $d + z_0$ and z.

Substituting the rearranged (19.1) and (19.16) for the canopy-scale energy balance equation, (19.15), and replacing the surface–air vapor pressure difference by the vapor pressure deficit of the ambient air (D_a), the equation for λE above the canopy, termed the Penman–Monteith (P-M) equation, is given by:

$$\lambda E = \frac{\Delta(R_n - G) + \rho_a c_p G_a D_a}{\Delta + \gamma(1 + (G_a/G_S))}, \tag{19.24}$$

where Δ is the rate of change of saturation water vapor pressure with temperature, and γ is the psychrometric constant (66.5 Pa K^{-1}). Equation (19.24) generally describes the transpiration stream from vegetation to the atmosphere. However, an infinite G_S represents no resistance between the canopy surface and within canopy, allowing (19.24) to derive evaporation from a free water surface, i.e., wet canopy evaporation.

When micrometeorological measurements including a measurement of H_2O exchange between the canopy and atmosphere (see Fig. 19.8a) are conducted, the only unknown variable in (19.24) is G_S. Thus, an inverted operation of (19.24) gives G_S (Fig. 19.8b) and enables us to examine the relationships between the G_S and various environmental factors (D_a in Fig. 19.8c). For example, using an analysis with (19.10) and procedures shown in Ewers et al. (2005) the relationship between the G_S and the D_a in Fig. 19.8c gives us important information on environmental and hydraulic control of G_S (see Fig. 19.3). Note that here G_S was calculated using the simplified form of the P-M equation (Monteith and Unsworth 2008) (detailed later).

19.6 Transpiration: Environmental Controls

When G_a is large enough that it can be assumed to be infinite, the canopy surface is well coupled to the atmosphere and the T_s tends to approach T_a. Then, we can obtain the imposed evaporation rate, E_{imp}, by setting G_a as infinity in (19.24):

$$E_{imp} = \frac{\rho_a c_p}{\lambda\gamma} G_S D_a. \tag{19.25}$$

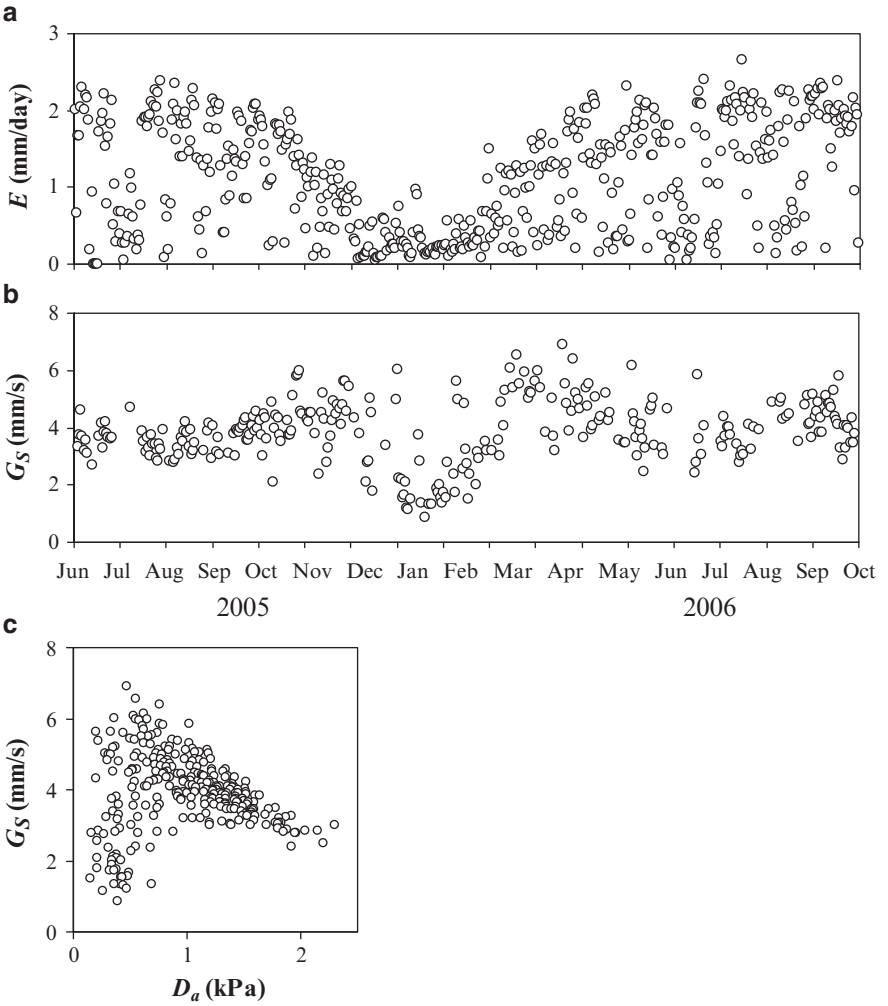

Fig. 19.8 Seasonal patterns of (**a**) daily canopy stand transpiration (E) and (**b**) daily canopy conductance (G_S), and (**c**) relationship between the G_S and atmospheric vapor pressure deficit (D_a) in a Japanese cedar forest

In this case, the evaporation is imposed by the atmosphere on the natural canopy surface through the effect of D_a, so that evaporation is proportional to the physiological conductance. Note that (19.25) is the simplified form of the P-M equation for a canopy that is well coupled with the atmosphere (Monteith and Unsworth 2008). On the other hand, when the G_a is very small, the canopy surface is poorly coupled with the atmosphere and evaporation tends to an equilibrium condition. In

this case, E is termed the equilibrium evaporation rate, E_{eq}, which can be obtained by substituting $G_a = 0$ for (19.24):

$$E_{eq} = \frac{\Delta(R_n - G)}{\lambda(\Delta + \gamma)}. \tag{19.26}$$

Equilibrium evaporation, E_{eq}, depends only on the energy supply (radiation) and is obtained over an extensive surface of uniform wetness.

The relative importance of radiative (E_{eq}) and advective (E_{imp}) energy for E (19.24) can be estimated using the equation (McNaughton and Jarvis 1983):

$$E = \Omega E_{eq} + (1 - \Omega)E_{imp}, \tag{19.27}$$

where the decoupling coefficient, Ω, is calculated as follows:

$$\Omega = \frac{\Delta/\gamma + 1}{\Delta/\gamma + 1 + g_a/g_c}. \tag{19.28}$$

The decoupling coefficient, Ω, is a measure of the coupling between conditions at the surface and those in the free air stream and can vary between 0 (for perfect coupling) and 1 (for complete isolation). Stomatal control of transpiration becomes progressively weaker as Ω approaches 1. It is apparent from (19.28) that Ω depends on the ratio between the surface conductance and that of the boundary layer, rather than on their absolute values (Jones 1992).

Observation in a Bornean tropical rainforest showed diurnal variations in E and their environmental control (Kumagai et al. 2004; Fig. 19.9). In this site, E had similar diurnal patterns to R_s, and estimates of Ω ranged from 0.1 to 0.4 and had no clear diurnal cycle.

19.7 Future Research Directions

Vegetation/forests cover a major part of the land surface and promote latent heat exchange as a result of transpiration. How the available energy is partitioned between sensible and latent heat fluxes at the air–land interface is critical for the formation of global and regional climate. In turn, the climatic modifications attendant on the alteration in land surface energy partitioning can impact forest transpiration due to a change in the environmental control. Also, it should be noted that subtracting evaporation from precipitation denotes the upper limit of available water resources for both humans and ecosystems.

The projected growth in atmospheric CO_2 will significantly increase global and regional temperatures with concomitant modifications to various climatic factors such

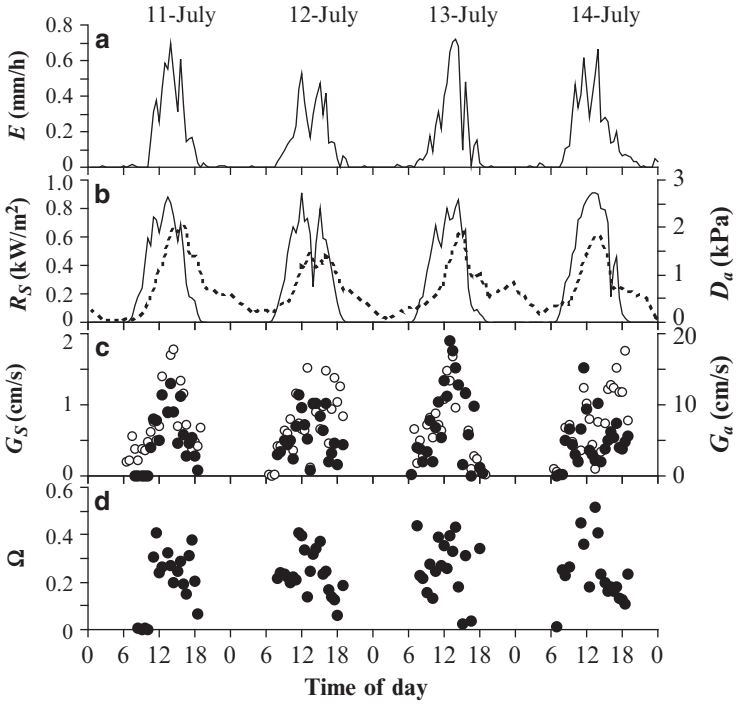

Fig. 19.9 Diurnal variations in (**a**) canopy transpiration (E), (**b**) solar radiation (R_s; *solid line*) and atmospheric vapor pressure deficit (D_a; *dashed line*), (**c**) canopy conductance (G_S; *solid circle*) and aerodynamic conductance (G_a; *open circle*), and (**d**) the decoupling coefficient (Ω; *solid circle*) observed in a Bornean tropical rainforest. From Kumagai et al. (2004), reproduced with permission

as atmospheric evaporative demand and precipitation patterns, and land use change accelerates these impacts. The climate and land use change factors alter forest transpiration by changes in ecophysiological characteristics of assimilation and transpiration as well as by those in the atmospheric evaporative demand. Furthermore, on much longer time scales, both spatial and temporal variations in physiological and morphological characteristics of plant species genotypically and/or phenotypically occur under climate change and could impact the exchange between forests and the atmosphere.

Thus, assessing the potential shifts in forest transpiration from both biological (stomatal opening, photosynthesis, hydraulic restriction in the stem xylem, and their genetic and/or nongenetic acclimation) and physical (surface energy balance, advection, convection, and atmospheric coupling) aspects is necessary for understanding climate change and quantifying local, regional, and global water cycling. Additionally, remote sensing technologies can serve among the most promising tool to investigate spatial impacts of climate and, especially, land use changes on the interaction between forests and the atmosphere.

References

Badger MR, Collatz GJ (1977) Studies on the kinetic machine of ribulose 1,5-bisphosphate carboxylase and oxygenase reaction, with particular reference to the effect of temperature on kinetic parameters. Carnegie Inst Washington Year Book 76:355–361

Baldocchi D (1992) A Lagrangian random-walk model for simulating water vapor, CO2 and sensible heat flux densities and scalar profiles over and within a soybean canopy. Bound Layer Meteorol 61:113–144

Ball JT, Woodrow IE, Berry JA (1987) A model predicting stomatal conductance and its contribution to the control of photosynthesis under different environmental conditions. In: Biggens J (ed) Progress in photosynthesis research. Mirtinus Nijhoff Publishers, The Netherlands, pp 221–224

Campbell GS, Norman JM (1998) An Introduction to Environmental Biophysics. Springer-Verlag, New York

Collatz GJ, Ball JT, Grivet C et al (1991) Regulation of stomatal conductance and transpiration: a physiological model of canopy processes. Agric For Meteorol 54:107–136

de Pury DGG, Farquhar GD (1997) Simple scaling of photosynthesis from leaves to canopies without the errors of big-leaf models. Plant Cell Environ 20:537–557

Ewers BE, Gower ST, Bond-Lamberty B et al (2005) Effects of stand age and tree species on canopy transpiration and average stomatal conductance of boreal forests. Plant Cell Environ 28:660–678

Farquhar GD, Wong SC (1984) An empirical model of stomatal conductance. Aust J Plant Physiol 11:191–210

Farquhar GD, von Caemmerer S, Berry JA (1980) A biochemical model of photosynthetic CO2 assimilation in leaves of C3 species. Planta 149:78–90

Jarvis PG (1976) The interpretation of the variations in leaf water potential and stomatal conductance found in canopies in the field. Philos Trans R Soc Lond Biol 273:593–610

Jones HG (1992) Plants and microclimate, 2nd edn. Cambridge University Press, Cambridge

Katul GG, Albertson JD (1999) Modeling CO_2 sources, sinks, and fluxes within a forest canopy. J Geophys Res 104:6081–6091

Kelliher FM, Luening R, Raupach MR et al (1995) Maximum conductances for evaporation from global vegetation types. Agric For Meteorol 73:1–16

Kumagai T, Saitoh TM, Sato Y et al (2004) Transpiration, canopy conductance and the decoupling coefficient of a lowland mixed dipterocarp forest in Sarawak, Borneo: dry spell effects. J Hydrol 287:237–251

Kumagai T, Aoki S, Nagasawa H et al (2005) Effects of tree-to-tree and radial variations on sap flow estimates of transpiration in Japanese cedar. Agric For Meteorol 135:110–116

Kumagai T, Ichie T, Yoshimura M et al (2006) Modeling CO2 exchange over a Bornean tropical rain forest using measured vertical and horizontal variations in leaf-level physiological parameters and leaf area densities. J Geophys Res. doi:10.1029/2005JD006676

Kumagai T, Aoki S, Shimizu T et al (2007) Sap flow estimates of stand transpiration at two slope positions in a Japanese cedar forest watershed. Tree Physiol 27:161–168

Kumagai T, Aoki S, Shimizu T et al (2008) Transpiration and canopy conductance at two slope positions in a Japanese cedar forest watershed. Agric For Meteorol 148:1444–1455

Leuning R (1995) A critical appraisal of a combined stomatal-photosynthesis model for C3 plants. Plant Cell Environ 18:339–355

McNaughton KG, Jarvis PG (1983) Predicting effects of vegetation changes on transpiration and evaporation. In: Kozlowski TT (ed) Water deficits and plant growth, vol V. Academic Press, New York, pp 1–47

Monteith JL, Unsworth MH (2008) Principles of environmental physics, 3rd edn. Academic Press, Oxford

Oren R, Sperry JS, Katul GG et al (1999) Survey and synthesis of intra- and interspecific variation in stomatal sensitivity to vapour pressure deficit. Plant Cell Environ 22:1515–1526

Tateishi M, Kumagai T, Utsumi Y et al (2008) Spatial variations in xylem sap flux density in evergreen oak trees with radial-porous wood: comparisons with anatomical observations. Trees 23:23–30

Umebayashi T, Utsumi Y, Koga S et al (2008) Conducting pathways in north temperate deciduous broadleaved trees. IAWA J 29:247–263

von Caemmerer S et al (1994) The kinetics of ribulose-1,5-bisphosphate carboxylase/oxygenase in vivo inferred from measurements of photosynthesis in leaves of transgenic tobacco. Planta 195:88–97

Watanabe T (1993) The bulk transfer coefficients over a vegetated surface based on K-theory and 2nd-order closure model. J Meteorol Soc Japan 71:33–42

Wilson NR, Shaw RH (1977) A higher order closure model for canopy flow. J Appl Meteorol 16:1198–1205

Wong SC, Cowan IR, Farquhar GD (1979) Stomatal conductance correlates with photosynthetic capacity. Nature 282:424–426